JJEES

JJEES (2025) 16 (4): 352-364
ISSN 1995-6681

Jordan Journal of Earth and Environmental Sciences

Petrography, Mineralogy, and Geochemistry of the Aïn Babouche ooidal ironstones (Northeastern Algeria): Implications for Depositional Environment, Iron Source and Ooids Formation.

Abdelhakim Bouchair[1,2*], Azzedine Bouzenoune[1,2], Chiara Benedetta Cannata[3], Mariano Davoli[3], Oumeima Benmebarek[1,2], Zoubir Belhimer[1,2]

[1]Geological Engineering Laboratory (LGG), University of Jijel, Central Campus, BP 98, 18000, Jijel, Algeria
[2]Department of Earth and Universe Sciences, Faculty of Natural and Life Sciences, University of Jijel, Central Campus, BP 98, 18000, Jijel, Algeria
[3]Center of Microscopy and Microanalysis – Department DiBEST of the University of Calabria, 87036 Arcavacata di Rende, Italy

Received on February 24, 2025, Accepted on May 6, 2025

Abstract

This study aims to examine the petrography, mineralogy, and geochemical characteristics of the Eocene ooidal ironstone formations at Aïn Babouche, located in the eastern part of the Saharan Atlas in order to determine the mechanism of ooid formation. The country rocks consist of Upper Cretaceous to Quaternary marls and limestones with a thickness of 6 Kilometres, while the iron-rich intervals (10 meters) are separated by centimetric levels of marl. These intervals are restricted to the Lutetian age. Petro-mineralogical investigations indicate that iron ore is composed mainly of ooids (goethite and limonite) and detrital minerals (quartz, clay, apatite). Geochemical analysis, using Laser Ablation Inductively Coupled Plasma Mass Spectrometry and X-ray fluorescence spectrometry, reflects the hydrogenous origin of the iron, more likely from a continental source, basinal brines, or a mixed source. The mechanism of ooid formation is suggested to be direct precipitation of iron around a nucleus in a shallow, agitated marine environment. This interpretation is based mainly on the sedimentological pattern and parameters, the ironstones, the morphology and internal geometry, and the composition of the ooids, as well as the associated framework components.

Keywords: *Ooidal ironstones; Eocene; Rare earth elements; Cerium anomaly; Ain Babouche; Algeria*

1. Introduction

The ooidal iron deposits were a significant source of iron that aided nineteenth-century industrial development (Petranek and Van Houten, 1997). In terms of iron resource richness, ooidal iron deposits rank after BIF-type deposits, which are related to magmatic processes. However, ooidal ironstone deposits are the most widespread globally, with almost 400 occurrences and total reserves estimated at over 66,000 million tonnes worldwide. As Petranek and Van Houten (1997) have demonstrated, ooidal ironstones are sandy, clayey, siliciclastic, or siliciclastic-carbonate sedimentary rocks that contain over 15% of iron. Furthermore, they have been observed to include more than 5% coated grains, which are oncoids, pisoids, and ooids (Salama et al., 2013). The investigation of ooidal ironstones can aid in reconstructing paleoenvironmental conditions and provide insights into the chemical and fluid dynamics within a basin.

Despite the research on ooidal ironstones, particularly marine ones, the genesis of these deposits is still debated, with explanations varying from deposit to deposit. Researchers have proposed various hypotheses that include the following: i) In 1856, Sorby proposed that ooids are formed by replacing calcareous ooids. This theory has garnered support from Kimberley (1979), Kearsley (1989), and Diab et al., (2020), who have provided substantial evidence in support of this assertion, including the presence of calcareous relics and early diagenetic siderite. ii) Intrasedimentary concretional growth as demonstrated by Hallimond (1951), Hemingway (1974), followed by Salama et al. (2014), Baioumy et al. (2017), and Garnit et al. (2017). Supporters of this theory have employed various methods to validate it, chiefly the presence of radial-fibrous concentric layers and the identification of authigenic minerals, such as siderite. iii) The extrasedimentary mechanical accretion of ooids (Bhattacharya & Kakimoto, 1982; Van Houten & Purucker, 1984; Kearsley, 1989). This one is supported by evidence such as well-rounded spherical ooids and the presence of sedimentary structures. iv) Dahanayake & Krumbein (1986) proposed the theory of primary biological accretion, which Burkhalter (1995) followed. The theory is supported by the presence of ferruginous stromatolitic microbialites that contain microbial laminae composed of fossilized leptothrix-like bacterial filaments (El Aref et al., 2006b; Salama et al., 2013, 2014). v) Siehl and Thein (1989) were the first to suggest that iron ooids or pisoids were derived from lateritic soils. This proposition was based on the absence of aluminium substitution and other evidence, which contradicted alternative theories. vi) Harder1989 proposed

* Corresponding author e-mail: Hakim.bouchair@univ-jijel.dz

crystallisation from precursor iron oxyhydroxide gels based on experimental or theoretical evidence that ferruginous gels can act as precursors to mineral phases, especially under early diagenetic conditions (low temperature and pressure).

In the African continent, ooidal ironstone deposits represent an important source of iron (McGregor et al., 2010), over 100 deposits are spread over six countries almost located in the north African basin (i.e. Algeria, Tunisia, Sudan, Morrocco, Libya, Egypt, and Nigeria), ranging in age from the Paleozoic (Ordovician to Devonian), Mesozoic (Jurassic and Cretaceous) to less commonly cenozoic (Petranek and Van Houten, 1997). In North Africa, only three Eocene ooidal ironstone occurrences have been inventoried: the Djebel Ank ooidal ironstone in central Tunisia, the Bahariya Depression in the Western desert of Egypt, and the Aïn Babouche in northeastern Algeria (Petranek and Van Houten, 1997; El Aref et al., 1999, 2006a, 2006b). The latter is considered "an uneconomic deposit", although it is currently mined, and the ore is used by cement factories in the region.

The Aïn Babouche ooidal iron deposit, hosted within Eocene formations, is the only deposit of this type currently mined in the Tebessa region. While the Tunisian Djebel Ank deposit, located approximately 160 km southeast, is equivalent to the Aïn Babouche deposit, as it is also hosted in Eocene formations (Garnit et al., 2017).

The purpose of the present study is to characterise the petrography, mineralogy, and geochemistry of the Eocene ooidal ironstones from the Aïn Babouche deposit in order to understand the sedimentation processes, depositional environment and diagenetic processes that prevailed during ironstone formation. It is hoped that this work can serve as a reference for studies of other ironstone deposits in different regions.

2. Geological background

The Aïn Babouche deposit is located in the north-east of Algeria, at a distance of 56 km south-west of the city of Tebessa and about 10 km west of the town of Telidjene (Figure 2). The Tebessa region is situated within the eastern Saharan Atlas, south of the Tell Atlas. It is separated from the Saharan platform to the south by the South Atlas Front, a structural alignment that extends over more than 1000 km. This alignment consists of a Palaeozoic basement covered by Meso-Cenozoic sediments (Figure 1). The main geological features of the Tebessa region include subsidence, diapirism, folding, faulting, and grabens. The sedimentary sequence thickness from the Barremian to the Quaternary is roughly 6 km, whereas bathymetric estimations do not surpass a few hundred meters (Dubourdieu, 1956).

The most ancient geological formations that outcrop in the Aïn Babouche sector are constituted of evaporitic rocks from the Triassic period mainly consisting of gypsum, variegated clays, cargneules, and dolomites. These rocks outcrop particularly to the NW and SE of the Aïn Babouche syncline in the Hamimat Guibeur and Hamimat Meskouta diapirs, respectively (Figure 2). Jurassic formations are absent from the outcrop. However, Vila (1992) reported the presence of exogenous Jurassic shreds of reduced size in the Triassic formations of the two diapirs.

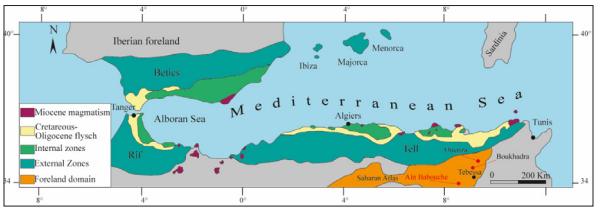

Figure 1. Map showing different domains of the Western Mediterranean Alpine orogen (modified from Durand Delga et Fontboté 1980; Vila, 1980; Etheve et al., 2016)

The Lower Cretaceous formations are limited to the central part of the Ain Telidjene anticline (Figure 2), represented by iron-bearing sandstones and dolomites. Limestones and dolomites, phosphate-bearing marls and brecciated limestones are often overlain by marly limestones.

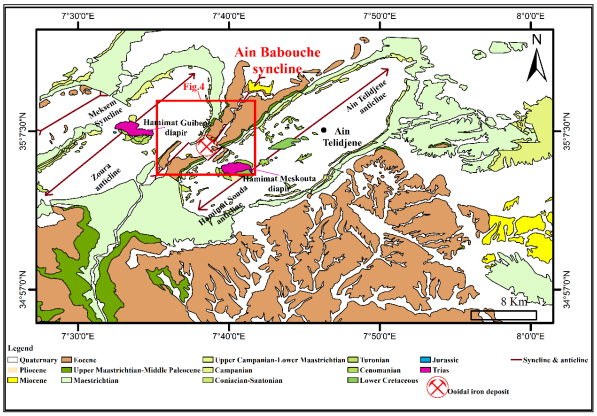

Figure 2. Geological sketch map showing the Aïn Babouche syncline among the so-called NE-SW "Atlasic folds" of the Northeastern Saharan Atlas of Algeria (Vila, 1992).

As stated by Vila (1992), the Upper Cretaceous formations are characterised by an alternation of gypsum marls and limestone. The Cretaceous successions consist mainly of limestones in the lower part and an alternation of limestones, marl and phosphatic rocks in the upper part (Figure 3). The Palaeocene formations consist of marls from the Dano-Montian period, with sedimentary continuity with those from the end of the Maastrichtian period. The Ypresian contains a series of limestones that include many multiform black or brown flints. They are rich in lumachellics shell debris and have a sparse cement with little phosphate debris.

Shown in Figure 4, stratiform ooidal ironstone layers are confined within the Lutetian series of partially ferrugenated marls, sandstones, and mudstone, topped by limestones and gypsum. Based on our geological cross-section and field observations (Figure 4), the mineralized zone consists of numerous layers of compact ooidal ironstones, totaling 11 layers. Due to their diminutive thickness, the ironstones mentioned above have been categorized into four primary layers in the cross-section. The stratigraphic sequence of the mineralised zone begins with an alternation of marls and ironstone, with a thickness range from 10-50 cm. The first levels of marls contain abundant debris of ostracodes, including several *NONIONELLASP AND VIRGULINA GR. DANVILLENSIS HOWE & WALLACE*, as well as *CAVERNOCYTHEREIS (LOXOCONCHA) CAVERNOSA*

(APOSTOLESCU & MAGNE). Based on the debris, Vila (1992) dated the series that contains the ooidal ironstones to the upper-middle Lutetian period. Thereafter, an alternation of thin layers of ironstone (5 to 10 cm) with layers of marl. The sequence concludes with two two-layer measuring 4 m in thickness. The ironstone layers show various sedimentary structures, includingcross-beddings, graded bedding, and channels (Figure 5). The cross-bedding is composed of bands with a thickness varying from 1.5 to 3 cm, separated by millimetre-sized laminae, consisting of consolidated iron oxide. The transition between the various formations exhibits no structures indicative of substantial modification. There are no structures of the emersion surface type, hardened surface, stratigraphic gap, or discordance.

The Miocene rocks consist mainly of siliceous conglomerates and a red sandy-clay series with rare carbonate elements (Figures 3 and 4).

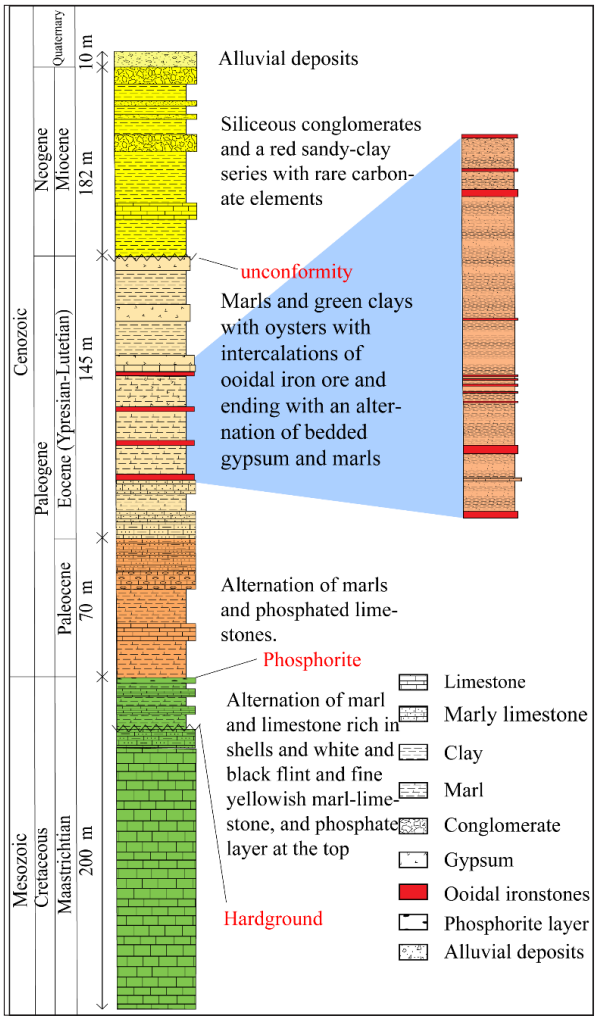

Figure 3. Litho-stratigraphic column of Djebel Dahar series (SE side of the Aïn Babouche syncline). Based on field and petrographical data, the chronological sequence was established by Vila (1992).

The Aïn Babouche region is marked by several folds and fault structures, some of which exhibit Triassic evaporitic rocks emplaced through multiphase diapiric activities (Figures 2 and 4). The fold structures consist of narrow synclines and wide anticlines with a NE–SW direction. They were formed during the Atlasic phase of the Upper Eocene, which affected the Saharan Atlas (Dubourdieu, 1956). The narrow Aïn Babouche syncline is located between the wide Zoura in the northwest side and the Aïn Telidjene anticline in the southeast side (Figure 4). The axis of the syncline (~10 x 3.5 km) aligns with the stream bed of the Wadi Babouche, trending NE–SW to the northeastern part, ENE–WSW to the central part, and NE–SW to the south-western part. The shift of directions is due to NW–SE faults that subdivide the syncline into three segments (Figure 4).

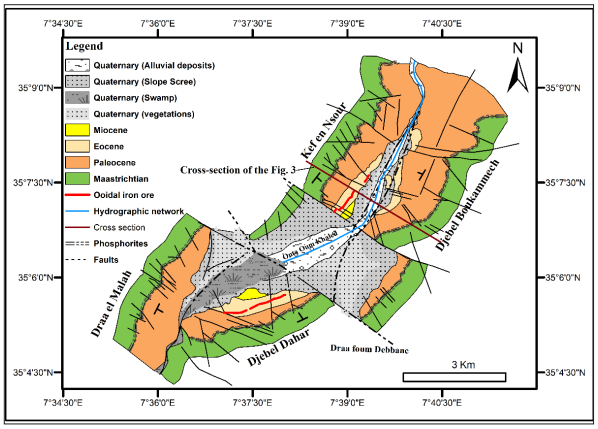

Figure 4. Geological map of the Aïn Babouche syncline showing the arrangement of the main iron ore outcrops within the different geological formations (Sonarem-Rudis, 1968; Keddar, 1985). (Extension of the ore body and Miocene formations were determined by the authors based on field observations and petrographical data).

3. Material and Methods

Sampling and field descriptions were carried out on the Aïn Babouche sedimentary series from both sides of the Aïn Babouche syncline. “Bed-by-bed” 37 samples were collected and described. Thin sections (90) and polished sections (20) were prepared in the geological engineering laboratory at the University of Jijel and in the laboratory of the geology department at the University of Annaba. They were examined using a Zeiss polarising and reflected light microscope, respectively.

X-Ray diffraction analysis (XRD) was performed at the Physitek Analysis and Equipment Laboratory using five bulk samples on a Smart Lab SE automated multipurpose X-ray diffractometer using Cu Kα radiation (λ = 1.5406 Å) with an accelerating voltage of 40 kV, a filament current of 40 mA, and a scan range between 5 and 70. Data were interpreted using X’Pert HighScore Plus software. Major element concentrations were also measured at Physitek Laboratory using an Epsilon 4 X-ray fluorescence spectrometer, operated at a tube voltage of 50 kV and a current of 1 mA.

Trace element (TE) analyses were carried out on eight polished sections, using the Laser Ablation Inductively Coupled Plasma Mass Spectrometry (LA-ICP-MS) at the Department of Earth Sciences “A. Desio” of the University of Milan, using an Analyte excite 193 nm ArF excimer laser coupled with an iCAP-RQ mass spectrometer. The operating conditions were 1 J/cm² fluence, a 65 µm spot size, and a 6 Hz repetition rate. The acquisition time was 60 seconds on the sample and 40 seconds on the background. Data reduction was performed using the software GLITTER (Griffin et al., 2008), with FeO wt% concentrations from the electron probe

micro-analyzer (EPMA) serving as an internal standard. The international reference material GSD-1g (Jochum et al., 2011) was used as the primary standard, and the reference glasses NIST 610, BCR-2g, and BHVO-2g (Jochum et al., 2011) were used to monitor accuracy.

Scanning electron microscopy (SEM), coupled with energy-dispersive X-ray spectroscopy (EDS) analysis, was performed on five polished and thin sections using a scanning electron microscope Ultra High-Resolution SEM (UHR-SEM) - ZEISS CrossBeam 350, coupled with an EDX spectrometer - EDAX OCTANE Elite Plus - Silicon drift type. The instrumental conditions set for the EDX analysis were as follows: HV, 15 keV; and probe current, 100 pA. The analyses SEM analyses were carried out at CM2 (Center of Microscopy and Microanalysis) – Department DiBEST (Biology, Ecology and Earth Sciences) of the University of Calabria, 87036 Arcavacata di Rende, Italy.

4. Results

4.1. Petrography

Petrographic examinations show that the ooidal ironstones of Ain Babouche Area are composed of more than 70% of ooids and granules as the main constituents of ironstones. Other grains are detritals, such as quartz (20%), phosphate (5%), glauconite, and other organic debris, which account for a small percentage. These components are set in a ferruginous clayey matrix and cemented by calcite cement.

The space between the ooids is filled by many grains; Quartz occupied the most space (Figure 6d), with rare apatite (Figure 8a), debris of carbonate organisms, including teeth probably belonging to “Selacians”, and the glauconite mentioned by Keddar (1985). In the flank of Kef en Nsour, the grains constituting iron ore are contiguous, unlike at Djebel Dahar, where they are spaced out from each other. The cement nature of Kef en Nsour ironstone is ferruginous or clayey, which explains the crumbly texture of the ore. In contrast, at Djebel Dahar, the deposit is larger due to the presence of carbonate cement.

Ooids are generally spherical, with a variable size (max 2 mm in diameter), and have a smooth outer surface under a reflected light microscope. The cores of the ooids are composed of goethite, while the concentric cortex consists of alternating colours between light and dark grey, corresponding to goethite and limonite, respectively (Figures 6 and 9). Each ooid typically has 2 to 10 concentric layers, with a thickness ranging from 50 µm to 200 µm. Most laminations are α-type (Figure 6a), which tend to regularise the morphology of the nucleus. In revanche, the β-type ooid is present in small quantities (Figure 6c) and tends to preserve the original morphology of the nucleus.

In addition to the ooids, granules are ubiquitously present in the iron ore. Granules are grains with the same composition as ooids but without the enveloping structures. In our case, they are mainly goethitic in composition and similar in size and shape to ooids (Figure 6d). The XRD analysis reveals that all the ooids and granules of the two flanks of the syncline of Ain Babouche (Kef en Nsour and Djebel Dahar) are both mainly composed of goethite (Figure 7).

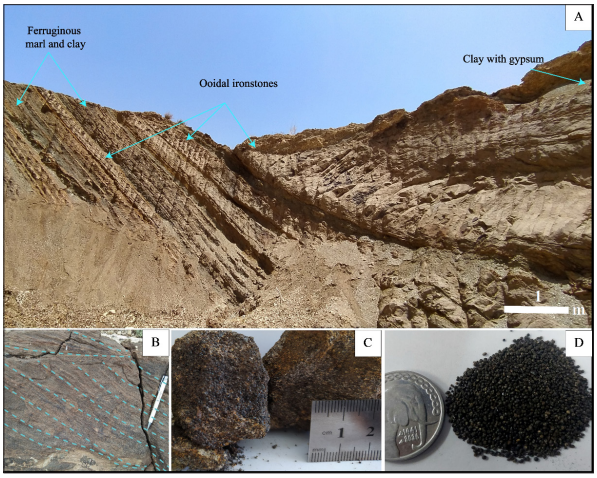

Figure 5. a) Field photos and macrophotographs illustrating the occurrence of two types of iron ore (ooidal ironstones and ferruginous marl and clay) at the scale of the outcrop. **b)** Ironstone layers with Cross-beddings. **c)** Ooidal ironstones. **d)** Crumbly sample ground by hand.

The nuclei of most ooids are typically rounded, which can be attributed to multiple phases of reworking. However, they rarely exhibit xenomorphic shapes (Figure 6a). Their diameter varies between 0.01 mm and 0.4 mm. Ooids typically consist of a single nucleus, although they may have up to four. Their composition might include quartz (Figure 8c), ooid fragments (Figure 6b), goethite fragments, and grains formed from a combination of several elements (quartz, goethite).

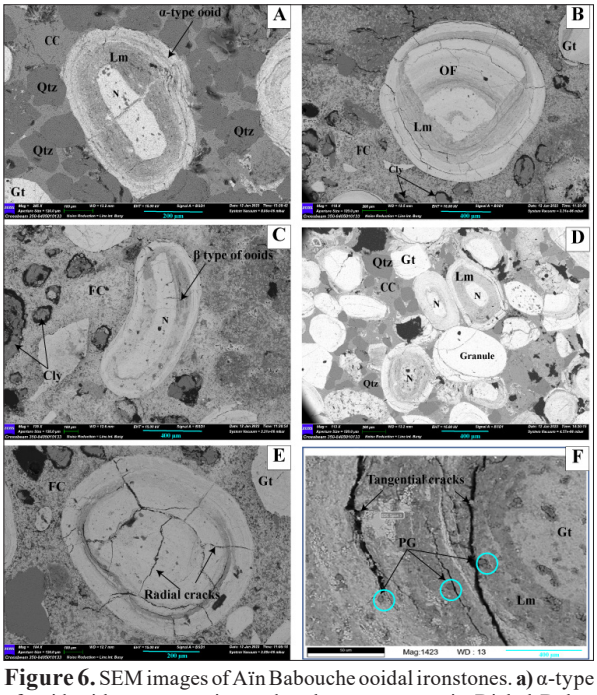

Figure 6. SEM images of Aïn Babouche ooidal ironstones. **a)** α-type of ooid with quartz grains and carbonate cement in Djebel Dahar ironstones. **b)** Ooid fragment as nucleus and clay grains cemented with a ferruginous cement in Kef en Nsour ironstones. **c)** β-type ooid with clay grains cemented with a ferruginous cement in Kef en Nsour ironstones. **d)** Ooids, granules, and quartz cemented with carbonate cement in Djebel Dahar ironstones. **e)** Ooid represents the radial type of cracks in Kef en Nsour ironstones **f)** The concentric layers of ooid contain phosphate grains. (Lm: limonite. Gt: Goethite Qtz: quartz. Ap: Apatite. Cly: Clay. PG: Phosphate grains. N: nucleus. CC: carbonate cement. FC: ferruginous cement. OF: ooid fragment)

Iron ooids have been identified as being affected by two distinct categories of cracks. (1) The most prevalent group of fractures is the early group, which is frequently oblique to parallel with the layers of the rim (Figure 8b). (2) The second group of cracks is radial to the various envelopes of the ooids. In certain instances, these cracks may divide the ooids into fragments, some of which serve as nuclei, leading to the formation of new layers of ooids around them (Figure 6b).

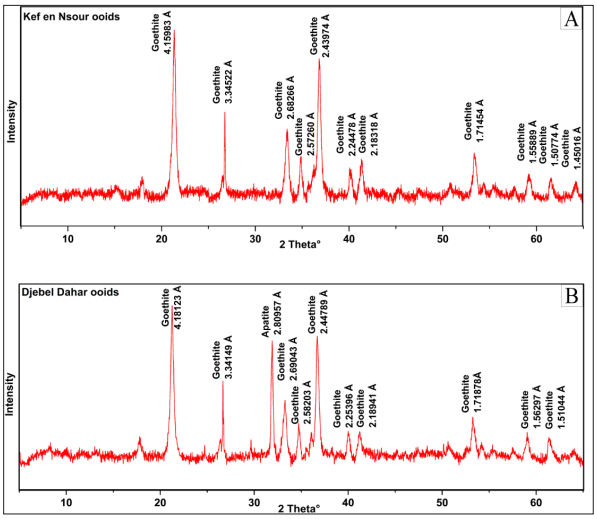

Figure 7. X-Ray diffractograms of two samples of ooidal ironstones (Ooids) showing the presence of goethite and Apatite minerals inside the ooids

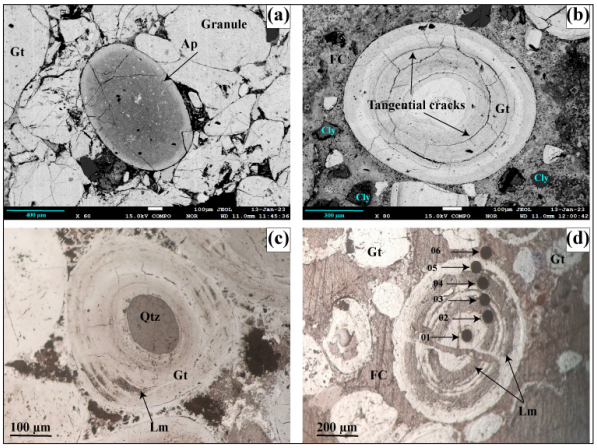

Figure 8. EMPA microphotographs of polished sections: **a)** Apatite grain with goethitic granules in Kef en Nsour ooidal ironstones. **b)** Ooid showing the tangential type of cracks in Kef en Nsour ooidal ironstones (Reflected light observation). **c)** Ooid with quartz nucleus. **d)** Ooid showing the LA-ICP-MS points analyses of the ooidal ironstone sample

4.3. Geochemistry

4.3.1. Major oxide elements

The concentrations of major oxides in the ooidal ironstones and the host rocks from Kef en Nsour and Djebel Dahar are shown in Table 1. In the iron ore, FeO is the most abundant, with an average (av.) content of (63.09 wt % FeO), followed by SiO_2 (av. 10.46 wt %) and Al_2O_3 (av. 3.64 wt %).

Table 1. Major oxides concentration (wt.%) of ooidal ironstones and host rocks of Kef en Nsour and Djebel Dahar (Aïn Babouche) measured by XRF (OI: Ooidal Ironstones, HR: Host Rocks; bdl = below detection limit)

Area	Samples	Rock type	SiO_2	Al_2O_3	FeO	CaO	MgO	MnO	K_2O	P_2O5	TiO_2
Djebel Dehar	DD01	OI	8.32	3.33	65.07	3.71	1.49	1.29	0.17	3.07	bdl
	DD06	OI	6.23	3.50	65.60	3.83	1.26	1.07	0.12	2.80	0.11
Kef en Nsour	ABW08	OI	9.05	3.40	63.45	1.33	0.76	0.87	0.13	1.92	bdl
	ABW09	OI	12.37	3.68	67.30	2.42	1.16	0.87	0.27	2.64	0.12
	ABW10	OI	8.13	3.29	61.07	0.49	0.96	0.10	0.13	1.17	0.09
	ABW10b	HR	50.12	7.58	5.24	1.57	0.27	bdl	1.31	0.18	0.75
	ABW11	OI	17.91	4.36	53.63	2.14	0.76	1.21	0.33	2.06	bdl
	ABW12	OI	13.22	3.59	58.42	6.35	1.23	1.41	0.23	5.13	0.15
	KN08	OI	8.47	3.99	70.22	0.92	1.16	0.92	0.12	1.72	bdl

The CaO concentrations (average 2.64 wt%), had a positive correlation with P2O5 (average 2.56 wt%), as expressed by a correlation coefficient of 0.98. The MgO content in ores varies from 0.76% to 1.49% (av. 1.09%). MnO content averages between 0.1% and 1.41%. TiO_2 and K_2O occur in very low proportions, with averages of 0.06% and 0.19%, respectively.

4.3.2. Trace elements

The trace element concentrations of the ooidal ironstones from Aïn Babouche were determined by LA-ICP-MS (Table 2). V and Zn recorded the highest concentrations among the trace elements, with an average of 682.88 ppm and 562.13 ppm, respectively. The average concentrations (ppm) of the other trace elements in descending order are Ni (332.45), Co (195.6), Cr (159.57), As (113.8), Ba (102.46), Sr (55.11), Pb (55.66), Y (50.09), Zr (35.85), Cu (10.17), Mo (9.5), U (9.24), Sc (8.06), Rb (7.92), Th (4.76), Nb (3.68), Sn (0.95), Sb (0.76), Hf (0.62), and Ta (0.12). The ooids of the two sides of the syncline (Kef en Nsour and Djebel Dahar) contain almost the same concentrations.

Upon normalization to the upper continental crust (UCC) as outlined by Taylor and McLennan, (1985), the concentrations indicate that V, Co, Ni, Zn, As, Mo, Ba, Pb, and Zn exhibit enrichment relative to the UCC. In contrast, Rb, Sr, Zr, Nb, Sn, Hf, and Ta demonstrate depletion (Figure 9). The same trends are observed in the ooidal ironstones on both the northwest flank (Kef en Nsour) and the southeast flank (Djebel Dahar). The same characteristics are observed in both the nuclei and the envelopes of the ooids.

Trace elements analysis of the Aïn Babouche ooidal iron deposit reveals significant similarities with regional and global ooidal iron deposits, including Djebel Ank (Tunisia, Garnit et al., 2017), Aswan (Egypt, Baioumy et al., 2017), and Bakchar (Siberia, Rudmin et al., 2019), as illustrated in Figure

10b. The slight differences include Sr depletion within Aïn Babouche ooids, whereas the ooids from Djebel Ank have higher contents of U and Mo. Additionally, samples from the Bakchar deposit exhibit higher concentrations of V and Ba, while showing lower contents of Co and Ni (Figure 9b).

Table 2. Aïn Babouche trace elements analysis of ooidal ironstones determined by LA-ICP-MS (values are the average of the measured points from the nucleus to the concentric layers for each sample)

	Djebel Dahar				Kef En Nsour			
Element (ppm)	STI04	DD01	DD06	STI01	ABW8	ABW9	ABW11	ABW12
Sc	8.42	8.07	7.75	8.61	7.79	8.20	7.36	8.29
V	798.97	606.85	713.43	806.66	594.46	569.24	644.36	729.10
Cr	151.56	87.08	208.37	187.58	159.69	124.51	206.13	151.66
Co	186.16	165.39	135.91	206.67	153.51	137.54	405.54	174.08
Ni	326.92	312.96	226.02	346.97	274.75	275.64	614.64	281.77
Cu	7.97	10.33	14.61	10.52	7.96	5.87	16.49	7.68
Zn	505.28	504.00	635.75	573.30	390.39	620.79	611.86	655.70
As	98.27	109.86	156.50	115.70	112.28	118.41	115.42	83.98
Rb	6.11	4.79	7.03	7.44	7.71	6.03	17.01	7.27
Sr	19.84	21.30	65.92	27.29	30.70	35.73	203.83	36.29
Zr	37.29	33.37	35.91	40.02	41.40	29.32	35.40	34.10
Nb	3.38	2.53	3.51	3.23	2.94	2.80	8.58	2.53
Mo	27.62	4.11	3.34	28.30	3.70	2.44	4.14	2.74
Sn	0.83	0.53	1.13	0.92	0.76	0.51	2.01	0.96
Sb	0.81	0.71	0.80	0.72	0.60	0.52	1.12	0.88
Ba	68.47	61.74	90.37	217.41	50.41	63.27	222.64	45.37
Hf	0.82	0.36	0.70	0.65	0.70	0.45	0.70	0.63
Ta	0.14	0.10	0.10	0.12	0.12	0.09	0.28	0.08
Pb	42.30	40.71	75.68	57.05	60.40	59.96	67.07	42.15
Th	4.56	2.58	5.72	5.65	4.97	3.32	5.54	5.83
U	10.67	7.73	11.18	10.28	13.41	7.34	7.25	6.13

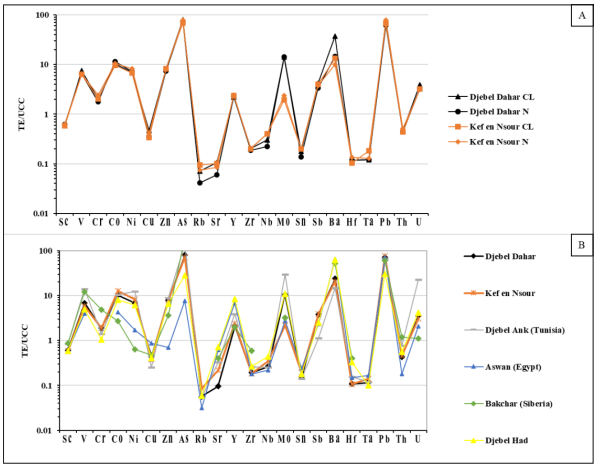

Figure 9. a) UCC-normalized trace elements of Aïn Babouche ooids nucleus (N) and the concentric layers (N). **b)** UCC-normalized trace elements of Aïn Babouche Fe ooids compared to Djebel Had deposit (Diab et al., 2020), Djebel Ank deposit (Garnit et al., 2017), Aswan deposit (Baioumy et al., 2017), and Bakchar deposit (Rudmin et al., 2019). Depleted values below 0.5 and those greater than two are enriched

The high content of Ni+Co and the low content of As+Cu+Mo+Pb+V+Zn mean that both Kef en Nsour and Djebel Dahar ooidal ironstone are within the hydrogenous fields of the binary diagram of trace elements. (Nicholson, 1992).

4.3.3 Rare earth elements

The total REE+Y content ranges between 104 and 362 ppm, with an average of 242 ppm (Table 3). The Kef en Nsour's average value of the total REE+Y (264 ppm) is slightly higher than that of Djebel Dahar's (220 ppm). The average value of the total REE+Y of 19 points analysed in the nucleus (244 ppm) is almost the same as the points in the concentric layers (221 ppm).

The patterns of REE values of Aïn Babouche ooidal ironstones normalised against post-Archean Australian shale (PAAS) (Taylor and McLennan, 1985) show a slight enrichment in HREE and MREE compared to LREE. The ores of the two flanks of the synclinal structure (Kef en Nsour to the NW and Djebel Dahar to the SE) show similar REE patterns (Figure 10a). In addition, similar REE patterns are also expressed in the nucleus and in the rim of the ooids analysed (Figure 10a).

The average ∑REE-Y values of Djebel Had (967 ppm), Aswan (631 ppm) (Baioumy et al., 2017), Djebel Ank (464 ppm) (Garnit et al., 2017), and Bakchar (399 ppm) (Rudmin et al., 2019) are all higher than the values of Aïn Babouche ironstone (242 ppm).

Figure 12 shows the patterns of REE values normalised against PAAS (Taylor and McLennan, 1985) of ooidal

ironstones of Aïn Babouche (Algeria), Djebel Had (Algeria, Diab et al., 2020), Djebel Ank (Tunisia, Garnit et al., 2017), Aswan (Egypt, Baioumy et al., 2017), and Bakchar (Siberia, Rudmin et al., 2019). Ironstones of Aïn Babouche have the same REE-Y signature as those of Djebel Ank and Aswan against PAAS. North African ooidal ironstones (Djebel Had, Djebel Ank, and Aswan) are slightly more enriched with heavy REE, unlike Bakchar ironstones, which are more enriched with light REE (Figure 10b). The North African ironstones also stand out from those of Bakchar by the presence of a positive cerium anomaly, which is absent in those of Bakchar.

Table 3. Aïn Babouche REE of ooidal ironstones determined by LA-ICP-MS analysis (values are the average of the measured points from the nucleus to the concentric layers for each sample)

	Djebel Dahar				Kef En Nsour			
Element (ppm)	STI04	DD01	DD06	STI01	ABW8	ABW9	ABW11	ABW12
La	23.59	33.39	9.37	22.13	34.05	18.81	23.72	10.52
Ce	93.13	101.60	29.92	92.77	109.22	61.46	174.43	34.15
Pr	7.58	8.90	3.63	7.54	11.54	6.11	9.66	4.18
Nd	29.83	34.64	14.74	30.10	49.37	24.79	43.94	16.64
Sm	6.99	7.94	4.67	7.77	12.30	6.52	11.34	5.03
Eu	1.95	1.97	1.42	2.11	3.34	1.79	3.16	1.51
Gd	8.75	7.60	5.86	8.52	14.70	8.04	12.17	7.06
Tb	1.63	1.33	1.21	1.68	2.41	1.24	2.18	1.30
Dy	10.78	8.26	7.70	11.38	16.52	9.32	12.32	9.05
Y	53.81	43.39	35.18	54.30	74.68	46.31	53.05	40.06
Ho	2.29	1.61	1.58	2.35	3.52	1.78	2.23	1.75
Er	7.26	5.65	4.41	6.59	9.79	5.52	6.56	5.35
Tm	1.06	0.84	0.77	1.06	1.32	0.84	0.94	0.83
Yb	7.11	6.28	4.78	6.80	9.15	5.66	6.12	5.59
Lu	1.01	0.85	0.75	0.94	1.24	0.75	0.86	0.64
∑REE-Y	256.77	264.25	104.99	256.06	353.13	198.94	362.68	143.67
LREE	171.82	196.04	58.01	170.95	234.51	127.53	278.42	79.09
HREE	84.95	68.21	46.97	85.11	118.62	71.42	84.26	64.58
Ce/Ce*	1.58	1.35	1.14	1.62	1.25	1.30	2.55	1.14
Eu/Eu*	1.16	1.18	1.27	1.21	1.16	1.16	1.26	1.18
Y/Y*	0.76	0.84	0.92	0.78	0.81	0.88	0.78	0.78
$Y_{(N)}/Ho_{(N)}$	0.87	1.00	0.83	0.85	0.78	0.97	0.88	0.85

The cerium anomaly Ce/Ce* = 2 $Ce_N/(La_N + Pr_N)$ was calculated according to De Baar et al. (1983). The europium anomaly was calculated as (Eu/Eu*) = $Eu_N/(Sm_N \times Gd_N)^{½}$ (Taylor and McLennan, 1985), and the yttrium anomaly as Y/Y* = $2Y_N/(Dy_N + Ho_N)$ (Fazio et al., 2007), where N is the normalised value. The ooidal ironstones of the Aïn Babouche deposit are characterised by a positive cerium anomaly for which Ce/Ce* varies from 1.14 to 2.55 and also a slight positive europium anomaly where Eu/Eu* is between 1.16 and 1.27. We note the presence of a slight negative yttrium anomaly where Y/Y* shows values between 0.76 and 0.92.

In the two discrimination diagrams of Bau et al., (2014) (Ce/Ce* vs Y_N/Ho_N) and (Ce/Ce* vs Nd), which are generally used for the discrimination between different genetic origins of ooidal ironstones, the samples from the iron ore of the Aïn Babouche deposit are plotted in the hydrogenous fields (Figure 13).

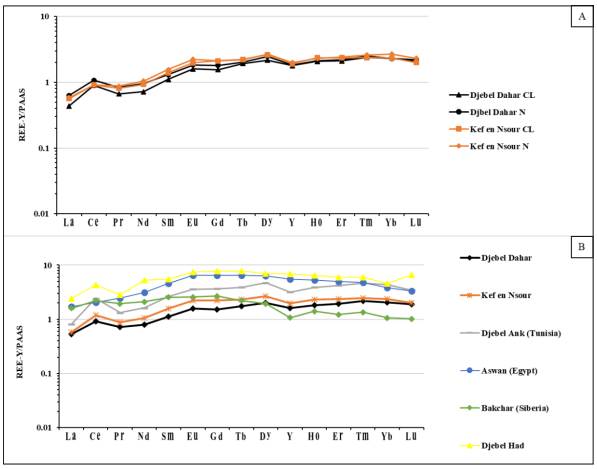

Figure 10. a) PAAS-normalized REE-Y of Aïn Babouche ooids nucleus and the concentric layers. **b)** PAAS-normalized REE-Y of Aïn Babouche iron ooids compared to Djebel Had deposit (Diab et al., 2020), Djebel Ank deposit (Garnit et al., 2017), Aswan deposit (Baioumy et al., 2017) and Bakchar deposit (Rudmin et al., 2019). Normalising factors inspired by Taylor and McLennan (1985).

4.3.4. Mineralogical and chemical variation in the ooids and their matrix

Maps of chemical element distribution (SEM-EDS) with punctual microanalyses are used in addition to EMPA analysis to confirm the microscopic observations of polished and thin sections. Iron is present in most of the ooids, granules, and some areas of the matrix (Figure 11c).

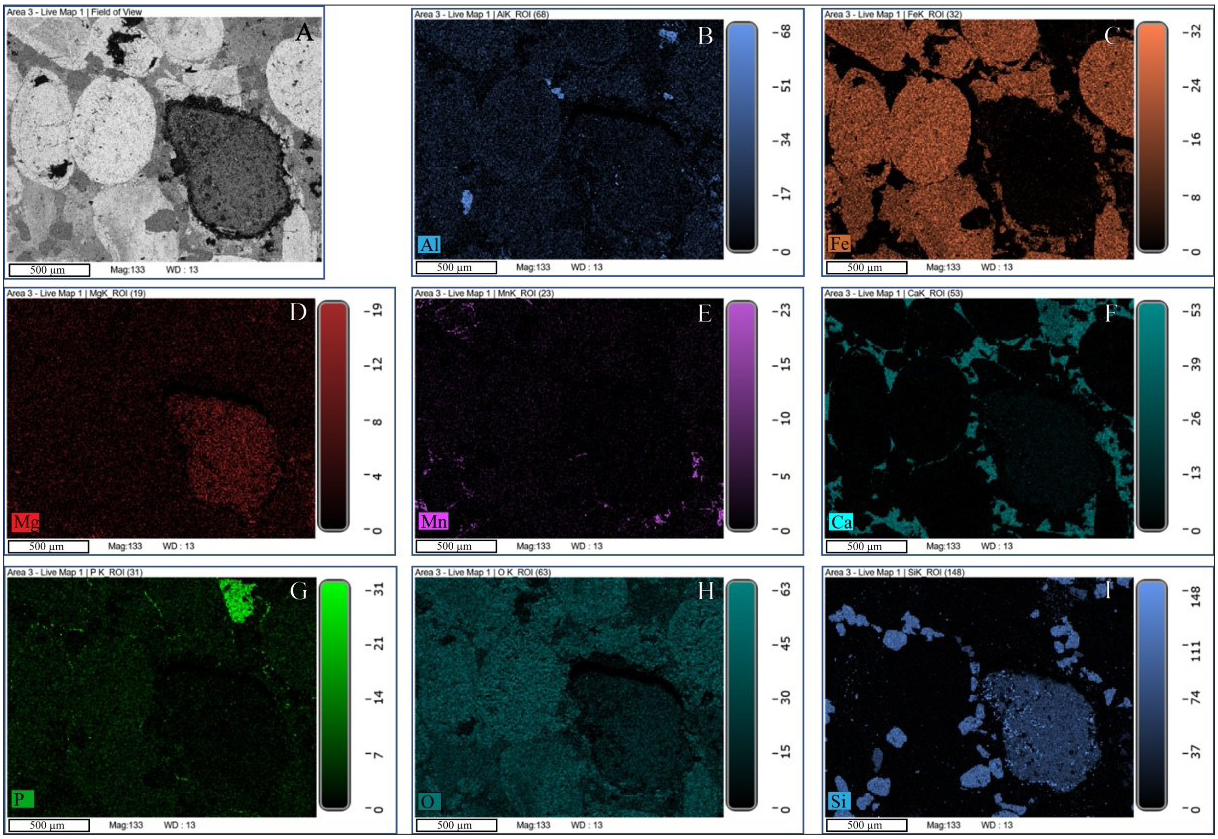

Figure 11. SEM-EDS maps of chemical element distribution

Al is particularly present in localised zones between oolitic grains, while Si is present only in quartz grains and in the grain to the right of Figure 10 a-i. The latter also contains an intermediate concentration of Mg and Al and is depleted in P and O (Figure 11b-d-g-h-i). Mn appears only in some small areas (Figure 11e). The concentration of P IS 0.9%. This element spreads across almost the entire area with low concentrations; however, in a small grain, it shows a high concentration (Figure 11g). Ca concentrations appear only in the matrix (Figure 11f).

5. Discussion

5.1. Petrography

The petrographic observation of Ain Babouche ooidal ironstones demonstrates the association of these iron ores with terrigenous and detrital minerals, including clay, quartz and apatite. This observation lends support to the hypothesis that the iron originated from a continental source. Sedimentary structures, such as metric cross-bedding, grading, and channelized facies, observed in the compact ooidal ironstones of Djebel Dahar (Figure 5b), argue for a relatively agitated shallow marine environment (e.g., Mutrux et al., 2008). This assertion is further substantiated by the observed correlation between the nucleus and the rim of the ooids, with the preponderance of α-type laminations (Figure 6a), suggesting that these ooids have formed in an agitated marine environment (Purser, 1980). In revanche, the β-type ooid is present in small quantities (Figure 6c), indicating formation in sheltered marine environments and non-marine caves (Purser, 1980). The nuclei of ooids are typically rounded, as Figure 6c shows, a consequence of multiple stages of reworking, and the majority of ooids exhibit a spherical to ellipsoidal shape, a result of the combined effects of accretion and corrosion (Scholle & Ulmer, 2003). Oblique cracks, parallel to the layers of the rim, are probably the result of compaction and retraction of ooids. The fragmented oolites indicate intense reworking and attest to an intensely agitated coastal palaeomilieu (Keddar, 1985). The presence of ooid fragments, sometimes constituting the nucleus of new ooids in the ironstones of Aïn Babouche, indicates intense reworking and serves as evidence of a shallow, intertidal, agitated environment. The angular shape of these fragments indicates that ooids have not been subjected to prolonged transportation.

Moreover, hydrothermal ooidal ironstones deposits are characterised by the presence of sulfide minerals, such as pyrite, chalcopyrite, sphalerite, galena, along with barite (Rudmin et al., 2019). Interestingly, our mineralogical examination reveals the absence of these minerals in the Ain Babouche ooidal ironstone, which allows us to distinguish it from hydrothermal ooidal ironstone deposits, as well as the metasomatic iron deposits of Ouenza and Boukhadra, located 100 km further north of Tebessa. The latter, as determined through stable isotope analysis and fluid inclusions (Bouzenoune et al., 1997; Bouzenoune et al., 2006;

Ait Abdelouahab et al., 2011; Bouzenoune, 2022), originate from the conversion of carbonate host rocks into iron ore, occurring at approximately 120 °C, with mineralising fluid salinities around 22% equivalent NaCl.

5.2. Geochemistry

In the Si-Al discrimination diagram of Choi and Hariya (1992) (Figure 12a), the Aïn Babouche iron ooids samples plot within the hydrogenous field, which is quite similar to Djebel Ank (Tunisia), Djebel Had (Algeria), and the Aswan deposit (Egypt), indicative of the same origin and formation process. This similarity is well supported in the diagram of Nicholson (1992) (Figure 12b), where all the Ain Babouche ironstone samples fall within the field of hydrogenous origin ores.

The strong positive correlation between CaO and P_2O_5 (i.e. 0.98), indicates that they originate from the same mineral phase, most likely apatite, which was also identified using SEM observations and elemental analyses (Figures 6f, 9a, and 10g). Moreover, the positive correlation between SiO_2 and Al_2O_3 confirms the presence of clay.

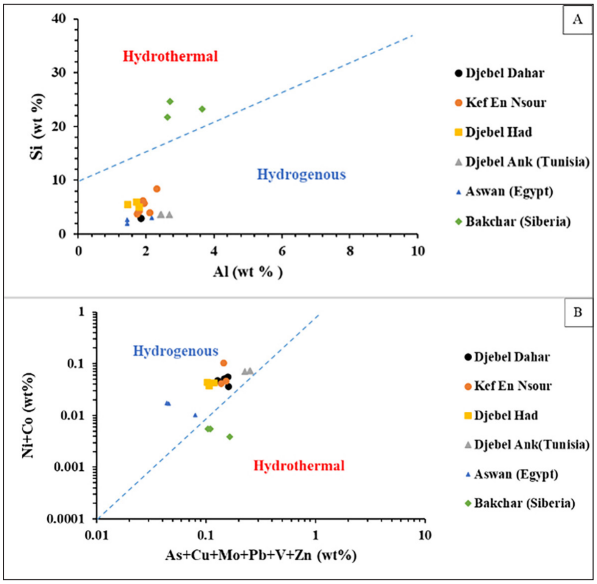

Figure 12. Cross plots between **a)** Si and Al by Choi and Hariya (1992); **b)** (Ni + Co) and (As + Cu + Mo + Pb + V + Zn) (Nicholson, 1992). Aïn Babouche values are compared to Djebel Had deposit (Diab et al., 2020), Djebel Ank deposit (Garnit et al., 2017), Aswan deposit (Baioumy et al., 2017) and Bakchar deposit (Rudmin et al., 2019)

Plotting the REEs in the two discrimination diagrams of Bau et al. (2014): Ce/Ce* vs. Nd and Ce/Ce* vs. YN/HoN (Figure 13a-b) reflects the hydrogenous origin of the iron in the studied deposits. The average value of the total REE+Y of 19 points analysed in the nucleus (244 ppm) is almost equivalent to the points in the concentric layers (221 ppm), suggesting no significant geochemical difference between the two mineralogical phases from which the nucleus is composed. In both cases, these phases consist of goethite. This similarity in composition is indicative of the identical genesis conditions of the ironstones on the two flanks of the syncline and also reflects the same origin for the two minerals (goethite) that constitute the nucleus and the cortex of the ooids.

Redox reactions likely control variations in cerium as Ce has two oxidation states, Ce^{3+} and Ce^{4+}. However, Ce^{4+} is almost never present in aqueous solutions unless strongly complexed in oxidising conditions (De Baar et al., 1983). The positive cerium anomaly and the negative yttrium anomaly in the ooidal ironstones of Aïn Babouche argue for environmental conditions rich in oxygen that prevailed in the Eocene Sea in which they were deposited. Under such oxidizing conditions, Ce^{3+} oxidizes and transforms into Ce^{4+}, which precipitates by being incorporated into different minerals such as the goethite ooids. It is important to acknowledge that the majority of authors who examined the ooidal ironstones of North Africa obtained analogous results and adopted the same interpretations (Salama et al., 2012; Garnit et al., 2017; Diab et al., 2020).

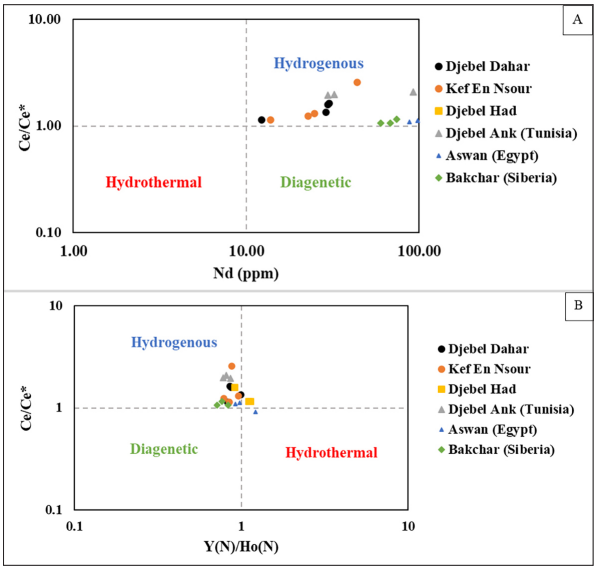

Figure 13. a) Ce/Ce* vs Nd discrimination diagrams. **b)** Ce/Ce* vs Y(N)/Ho(N) discrimination diagrams Bau et al., (2014). Aïn Babouche values are compared to Djebel Had deposit (Diab et al., 2020), Djebel Ank deposit (Garnit et al., 2017), Aswan deposit (Baioumy et al., 2017) and Bakchar deposit (Rudmin et al., 2019)

The study of Ain Babouche ooidal ores using SEM revealed that ooids are devoid of any discernible precursor carbonate or clay minerals, suggesting that goethite formation is not attributable to replacement processes. Furthermore, observations indicated that calcite was exclusively present as cement between the ooids and the granules, with no indication of replacement by iron-bearing minerals (Figure 6d). The presence of Al is particularly evident in localised zones between oolitic grains, suggesting the possibility of clay minerals. Conversely, Si is present only in quartz grains and in the grain located to the right of Figure 10a. The observed concentrations of Mg and Al in certain grains indicate the presence of clay minerals (Figure 11b-d-g-h-i). These findings collectively support the hypothesis of a continental source of iron, characterised by terrigenous and detrital minerals. The presence of Mn is only observed in specific areas, which may be indicative of rare grains of manganese minerals such as cryptomelane and psilomelane, as reported by Diab et al. (2020) in the Aïn Babouche deposit and by Garnit et al. (2017) in the Djebel Ank deposit (Figure 11e). The presence of elevated phosphorus concentrations in small grains is indicative of apatite (Figure 11g).

5.3. Depositional environment

The depositional environment of the North African Eocene ooidal ironstones is believed to be a shallow intertidal setting. This interpretation is mainly supported by the presence of sedimentary structures such as cross-bedding, the size and shape of grains, and petrographic features such as the presence of authigenic minerals (El Aref et al., 2006a; Salama et al., 2012; Garnit et al., 2017; Diab et al., 2020), and the presence of some microbial structures that develop in calm water conditions (El Aref et al., 2006b).

The border region between Algeria and Tunisia is situated on an epineritic platform, where the island of Kasserine developed from the late Cretaceous to the Miocene (Chabou-Mostefai et al., 1978; Zaïer et al., 1998). Significant phosphorite deposits, currently being exploited in Algeria and Tunisia, were formed around this island during the late Palaeocene to Early Eocene in a shallow intertidal depositional environment (Kechiched et al., 2016; Dassamiour et al., 2021). The Eocene ironstone deposits of Aïn Babouche (Algeria) and Djebel Ank (Tunisia) were formed under these palaeogeographic conditions. They are located to the west and south of the island, respectively. The high phosphate contents in the ironstones at Aïn Babouche likely originate from nearby phosphorite deposits situated approximately 50 km to the southeast (Djebel Onk phosphate deposits) and northeast (Kouif and Djebel Dyr phosphate deposits) of the Aïn Babouche ironstone deposit.

The presence of sedimentary structures such as metric cross-bedding and channelized facies indicates a marine environment that was likely to be shallow and agitated. The presence of laminations (alpha type with some beta type) indicates agitation, as do spherical to ellipsoidal shapes (due to accretion/corrosion). Ooid fragments sometimes form the nucleus of new ooids, showing intense reworking and confirming a shallow, agitated intertidal environment.

5.4. Source of iron

In the genetic models employed in the studies that addressed the Cenozoic ooidal iron deposits, three primary sources of iron were suggested: a continental source by alteration of pre-existing rocks, a hydrothermal source involving iron-rich fluids, and a mixed source with continental weathering and hydrothermal contribution (Young, 1989; Salama et al., 2012; Baioumy et al., 2017; Garnit et al., 2017; Rudmin et al., 2019; Diab et al., 2020).

The most common conclusion of previous studies is that the continental source is the most probable. For the Djebel Ank ironstone deposit, Garnit et al., (2017) posit a continental source for several reasons, including the relatively high content of phosphorus (up to 2%) and the low TiO_2/Al_2O_3 ratio (0.2–0.3). The authors considered that phosphorus and iron are usually believed to be transported to the basin of deposition after being leached from a continental source. Similarly, at the Djebel Had deposits, Diab et al. (2020) believe that iron is leached from the adjacent metasomatic continental formations associated with diapirism. However, they do not give any information on these metasomatic rocks. The authors approve their conclusion on indirect arguments, including mineralogical evidence, such as the presence of piemontite and pyrochlore in the ironstones, and geochemical evidence, such as the abundance of As, Zn, and Ag and the low content of Eu, which rules out a hydrothermal source of iron.

Many studies have considered a hydrothermal source of the iron of the ooidal ironstones (Villain, 1902; Schweigart, 1965; Kimberley, 1989; Rudmin et al., 2019). This hypothesis suggests that the precipitation of iron occurs from Fe-rich fluid flux or hydrothermal fluid with or without the intervention of volcanic events. The main arguments used to support this hypothesis include the concentrations of trace elements such as Pb, Cu, Zn, As, Bi, Ti, Cr, Mo, Li, and B that concentrate only in hydrothermal fluids (Schweigart, 1965); REE such as positive anomalies of Eu; and some mineralogical evidence, such as the presence of authigenic minerals. In contrast, several authors (Salama et al., 2012; Baioumy et al., 2017; Garnit et al., 2017) consider a hydrogenous source of iron based on trace elements and REE discrimination diagrams. The dehydration and crystallization of this gel yields iron hydroxide. In the case of ironstones from the Aïn Babouche deposit, and with reference to the results obtained in this study, it would appear that most of the results, and in particular the geochemical data, point to a hydrogenous origin for the ores from this deposit. Moreover, a mixed source of iron has been proposed by Baiyoumi et al. (2014) and Rudmin et al. (2019), combining hydrothermal and continental sources.

The hypothesis of a continental source for the iron in the ores from the Aïn Babouche deposit is supported by the deposition of ooids in a shallow, agitated marine environment near continental margins, alongside the association of these iron ores with terrigenous and detrital minerals, including clay and quartz, in addition to their geochemical characteristics. However, the palaeogeography of the Eocene period does not allow us to identify any rocks likely to have supplied, through supergene alteration, such large quantities of iron as would be required to form a deposit of around 10 million tonnes, such as that at Aïn Babouche.

On the other hand, the mobilization of iron from ante-Eocene sedimentary series, dominated by clay and marl by relatively saline hydrothermal fluids and its introduction into the marine environment, remains plausible. The Hamimat Guibeur and Hamimat Meskouta diapirs, located respectively to the northwest and southeast of the Aïn Babouche deposit (Figure 2), would play a significant role in providing the heat and salinity, enabling the basinal fluids to acquire the capacity to dissolve the iron contained in the ante-Eocene sedimentary series and creating a favourable geo-tectonic context for the circulation of hydrothermal fluids (Bouzenoune et al., 1995; Bouzenoune, 2024). It is also interesting to note that the structure of the Aïn Babouche deposit is strongly compartmentalised by tectonic accidents in an NW–SE direction (Figure 4) and that the three main outcrops of diapiric Triassic evaporites are aligned along one of these strike-slip tectonic accidents with a sinistral component (Draa Foum Debbane strike-slip fault, Figure 4). This accident was also considered as a portion of a long

lineament (Gafsa fault or Khenchela–Tripolitania lineament) along which the deposits of Aïn Babouche and Djebel Ank are located, as well as other deposits (Nicolini, 1967; Vila, 1992).

5.5. Formation of ooidal ironstones

The formation of the iron ooids that constitute ironstone-type deposits has been the subject of numerous scientific studies, and various mechanisms have been proposed to explain the genesis of these ooids (Sorby, 1856; Hemingway, 1974; Kimberley, 1979; Van Houten and Purucker, 1984; Harder, 1989; Siehl and Thein, 1989; El Aref et al., 2006b; Salama et al., 2012; Garnit et al., 2017; Rudmin et al., 2019). One of the most frequently invoked mechanisms is that proposed by Sorby (1856), which stipulates the transformation of carbonate ooids into iron ooids following the percolation of iron-rich fluids into the surrounding rocks. This mechanism has also been used to explain the genesis of the ooids in the Djebel Had deposit, which is part of the Aïn Babouche deposit (Diab et al., 2020). The results obtained from the study of the Kef en Nsour and Djebel Dahar ores showed that calcite was observed only as a cement between the ooids and granules, with no trace of possible replacement by iron-bearing minerals (Figure 6d). In addition, SEM observation of the ooids showed no trace of any precursor carbonate or clay minerals at the expense of the goethite that may have been formed by replacement. Microchemical analyses of the ooids showed relatively low Ca and Al contents (average of 0.26 wt % and 1.65 wt %, respectively), reflecting the absence of carbonate or clay minerals together with the non-existence of calcareous ooids in the surrounding area indicative of possible precursors replaced by goethite.

The spherical shape of ooids is a result of the combined effect of accretion and corrosion, in addition to the presence of ooid cracks, ooid fragments, and rounded nuclei, which are characteristics of multiple stages of reworking. The concentric laminae provide support for accretionary growth. Furthermore, the existence of modern analogue like the ongoing formation of iron ooids on the island of Panarea in Italy (Di Bella et al., 2019) and the unconsolidated submarine deposit of iron ooids and pisoids on the volcanic island of Mahengetang, Indonesia (Heikoop et al., 1996), can provide physical evidence of the chemical precipitation of iron around seafloor particles and that can be observed almost in real time.

In summary, Whether the source of the iron is continental, hydrothermal, or mixed, once introduced into the marine environment, the iron undergoes oxidation from the soluble and mobile ferrous state (Fe^{2+}) to the ferric state (Fe^{3+}), leading to precipitation. Oxidising conditions, expressed by the positive cerium anomaly, result from exchanges between the atmosphere and marine waters, producing an increase in the quantity of dissolved oxygen and, consequently, the oxidation of Fe^{2+} to Fe^{3+} and its precipitation in the form of a ferrihydrite gel. In the case of the introduction of bivalent iron (Fe^{2+}) dissolved in the marine environment in the form of $FeCl_2$ from basinal brines and continental supplies, the iron hydroxide gel (ferrihydrite) that precipitates following the oxidation of the bivalent iron is transformed into much more stable phases such as goethite and hematite (Pedersen et al., 2005; Benderev et al., 2022). The stable goethite precipitate directly around seafloor particles in a shallow, agitated marine environment.

6. Conclusion

This study investigates the petrographic, mineralogical, and geochemical characteristics of the ooidal ores of the Aïn Babouche deposit. The following conclusions arise:

Sedimentary structures such as cross-bedding, grading, and channelized facies, as well as the fragmented state of the ooids whose fragments constitute the nuclei of other, more recent ooids, argue for a shallow and relatively agitated marine environment. The geochemistry of the major elements and the trace elements in the ironstones indicates the hydrogenous origin of the iron. Two potential sources of iron have been suggested. The iron could be leached from a continental source, or the iron could come from basinal brines. A mixed source is also plausible.

The genesis of the ooids of Aïn Babouche was eceded by the saturation of iron in water, which was achieved by the fluvial flow of continental origin and/or by leaching of the ante-Eocene series by basinal brines. Subsequently, iron (Fe^{2+}) oxidizes and precipitates as a low-crystalline ferrihydrite gel, which is transformed by oxidation into more stable phases that precipitate around solid particles in a shallow, agitated marine environment.

References

Ait Abdelouahab, Dj., Bouzenoune, A., Préat, A. (2011). Les isotopes stables du carbone et de l'oxygène des carbonates (calcaires et sidérites) du gisement de fer de Boukhadra (Algérie nord orientale). Bulletin du Service Géologique National 22 : 381-395.

Baioumy, H., Omran, M., Fabritius, T. (2017). Mineralogy, geochemistry and the origin of high-phosphorus oolitic iron ores of Aswan, Egypt. Ore Geology Reviews 80: 185-199. https://doi.org/10.1016/j.oregeorev.2016.06.030

Bau, M., Schmidt, K., Koschinsky, A., Hein, J., Kuhn, T., Usui, A. (2014). Discriminating between different genetic types of marine ferro-manganese crusts and nodules based on rare earth elements and yttrium. Chemical Geology 381: 1-9. https://doi.org/10.1016/j.chemgeo.2014.05.004

Benderev, A., Trayanova, M., Tarassov, M., Tarassova, E. (2022). Conditions and processes of precipitation of iron compounds upon discharge of high-mineralised artesian water from artesian borehole R-30, Staro Oryahovo, Bulgaria. Environ Geochem Health 44: 2235-2251.https://doi.org/10.1007/s10653-021-01107-6

Bhattacharya, D.P., Kakimoto, P.K. (1982). Origin of ferriferous ooids: an SEM study of ironstone ooids and bauxite pisoids. Journal of Sedimentary Petrology 52: 849-857.

Bouzenoune, A., Rouvier, H., Thibieroz, J. (1995). Trias de l'Ouenza : context diapirique, zonation minéralogique et conséquences métallogéniques. Bulletin du Service Géologique de l'Algérie 6 : 3-24.

Bouzenoune, A., Rouvier, H., Thibieroz, J. (2006). Chronologie relative et conditions de mise en place des minéralisations du massif de l'Ouenza (Algérie NE). Bulletin du Service Géologique de lɔAlgérie 17 : 3-27.

Bouzenoune, A. (2022) Salt Tectonics and Mineralization Processes in NE Algeria. In: Meghraoui, M., Sundararajan, N.,

Banerjee, S., et al. (Eds.), Advances in Geophysics, Tectonics and Petroleum Geosciences. Springer International Publishing, Cham, pp. 623–626 https://doi.org/10.1007/978-3-030-73026-0_138

Bouzenoune, A. (2024). Petrographic and Geochemical Particularities of the NE Algerian Salt Domes and Associated «Cap-Rocks,» in: Khomsi, S., Bezzeghoud, M., Banerjee, S., Eshagh, M., Benim, A.C., Merkel, B., Kallel, A., Panda, S., Chenchouni, H., Grab, S., Barbieri, M. (Eds.), Selected Studies in Geophysics, Tectonics and Petroleum Geosciences, Advances in Science, Technology & Innovation. Springer Nature Switzerland, Cham, pp. 205–208. https://doi.org/10.1007/978-3-031-43807-3_43

Bouzenoune, A., Lécolle, P. (1997). Petrographic and geochemical arguments for hydrothermal formation of the Ouenza siderite deposit (NE Algeria). Mineralium Deposita 32 : 189-196. https://doi.org/10.1007/s001260050084

Burkhalter, R.M. (1995) Ooidal ironstones and ferruginous microbialites: origin and relation to sequence stratigraphy (Aalenian and Bajocian, Swiss Jura mountains). Sedimentology 42 : 57-74.

Chabou-Mostefai, S., Devolve, J.J., Fuchs, Y., Menant, G., Reviere, M. (1978). Sur les niveaux à célestite de Tunisie centrale et du Sud-constantinois. Sciences de la Terre 22 : 291-300.

Choi, J.H., Hariya, Y. (1992). Geochemistry and depositional environment of Mn oxide deposits in the Tokoro Belt, northeastern Hokkaido, Japan. Economic Geology 87: 1265-1274. https://doi.org/10.2113/gsecongeo.87.5.1265

Dahanayake, K., Gerdes, G., Krumbein, W.E. (1985). Stromatolites, oncolites and oolites biogenically formed in situ. Naturwissenschaften 72: 513-518.

Dassamiour, M., Mezghache, H., Raji, O., Bodinier, J.-L. (2021). Depositional environment of the Kef Essennoun phosphorites (northeastern Algeria) as revealed by P2O5 modeling and sedimentary data. Arabian Journal of Geosciences 14: 1-17. https://doi.org/10.1007/s12517-021-07400-z

De Baar, H.J.W., Bacon, M.P., Brewer, P.G. (1983). Rare-earth distributions with a positive Ce anomaly in the Western North Atlantic Ocean. Nature 301 : 324-327. https://doi.org/10.1038/301324a0

Di Bella, M., Sabatino, G., Quartieri, S., Ferretti, A., Cavalazzi, B., Barbieri, R., Foucher, F., Messori, F., Italiano, F. (2019). Modern Iron Ooids of Hydrothermal Origin as a Proxy for Ancient Deposits. Scientific Reports 9, 7107. https://doi.org/10.1038/s41598-019-43181-y

Diab, H., Chouabbi, A., Chi Fru, E., Nacer, J.-E., Krekeler, M. (2020). Mechanism of formation, mineralogy and geochemistry of the ooidal ironstone of Djebel Had, northeast Algeria. Journal of African Earth Sciences 162: 103736. https://doi.org/10.1016/j.jafrearsci.2019.103736

Dubourdieu, G. (1956). Etude Géologique de la Région de l'Ouenza (Confins Algéro-Tunisiens). Paris University, France.

Durand-Delga, M. and Fontboté, J.M. (1980). Le cadre structural de la Méditerranée occidentale. In: Aubouin, J., Debelmas, J., and Latreille, M. (Eds.), Géologie des chaînes alpines issues de la Téthys, Colloque No. 5, 26th International Geological Congress, Paris, Mémoires du Bureau de Recherches Géologiques et Minières 115: 67-85.

El Aref, M.M., El Sharkawi, M.A., Khalil, M.A. (1999). Geology and genesis of the strata-bound and Stratiform Cretaceous–Eocene iron ore deposits of the Bahariya region,Western Desert, Egypt. GAW 4th Int. Conf., Cairo Univ., Egypt, pp. 450-475.

El Aref, M.M., Mesaed, A.A., Khalil, M.A., Salama, W.S. (2006a). Stratigraphic setting, facies analyses and depositional environments of the Eocene ironstones of Gabal Ghorabi mine area, El Bahariya Depression, Western Desert, Egypt. Egyptian Journal of Geology 50: 29-57.

El Aref, M.M., Mesaed, A.A., Khalil, M.A., Salama, W.S. (2006b). Microbialite morphostructures and biogenic accretion mechanism of the Eocene ironstones of Gabal Ghorabi mine area, El Bahariya Depression, western Desert, Egypt. Egyptian Journal of Geology 50: 59-81.

Etheve, N., de Lamotte, DF., Mohn, G., Martos, R., Roca, E., Blanpied, C. (2016). Extensional vs. contractional Cenozoic deformation in Ibiza (Balearic Promontory, Spain): integration in the West Mediterranean back-arc setting. Tectonophysics 682: 35–55.

Fazio, A.M., Scasso, R.A., Castro, L.N., Carey, S. (2007). Geochemistry of rare earth elements in early-diagenetic miocene phosphatic concretions of Patagonia, Argentina: Phosphogenetic implications. Deep Sea Research Part II 54: 1414-1432. https://doi.org/10.1016/j.dsr2.2007.04.013

Garnit, H., Bouhlel, S. (2017). Petrography, mineralogy and geochemistry of the Late Eocene oolitic ironstones of the Jebel Ank, Southern Tunisian Atlas. Ore Geology Reviews 84: 134-153. https://doi.org/10.1016/j.oregeorev.2016.12.026

Griffin, W.L., Powell, W.J., Pearson, N.J., O›Reilly, S.Y. (2008). GLITTER: data reduction software for laser ablation ICP-MS: laser Ablation-ICP-MS in the earth sciences. Mineralogical Association of Canada Short Course Services 40: 204-207.

Gross, G.A. (1965). Geology of iron deposits in Canada, V 1., Geological Survey of Canada, Canada.

Hallimond, A.F. (1951). Problems of the Sedimentary Iron Ores. Proceedings of the Yorkshire Geological Society 28: 61-66.

Harder, H. (1989). Mineral genesis in ironstones: a model based upon laboratory experiments and petrographic observations. Geological Society, London, Special Publications 46: 9-18. https://doi.org/10.1144/GSL.SP.1989.046.01.04

Hemingway, J.E. (1974). Jurassic, in: The Geology and Mineral Resources of Yorkshire, edited by Raynor, D.H., Hemingway, J.E. Yorkshire Geological Society, London. pp.161-223.

Heikoop, J.M., Tsujita, C.J., Risk, M.J., Tomascik, T., Mah, A.J. (1996). Modern iron ooids from a shallow-marine volcanic setting: Mahengetang, Indonesia. Geology 24: 759. https://doi.org/10.1130/0091-7613(1996)024<0759:MIOFAS>2.3.CO;2

Jochum, K.P., Weis, U., Stoll, B., Kuzmin, D., Yang, Q., Raczek, I., Jacob, D.E., Stracke, A., Birbaum, K., Frick, D.A., Günther, D., Enzweiler, J. (2011). Determination of Reference Values for NIST SRM 610–617 Glasses Following ISO Guidelines. Geostandard Geoanalytic Research 35: 397-429. https://doi.org/10.1111/j.1751-908X.2011.00120.x

Kearsley, A.T. (1989). Iron-rich ooids, their mineralogy and microfabric: clues to their origin and evolution. Geological Society, London, Special Publications 46: 141-164. https://doi.org/10.1144/GSL.SP.1989.046.01.14

Kechiched, R., Laouar, R., Bruguier, O., Laouar-Salmi, S., Ameur-Zaimeche, O., Foufou, A. (2016). Preliminary Data of REE in Algerian Phosphorites: A Comparative Study and Paleo-redox Insights. Procedia Engineering 138: 19-29. https://doi.org/10.1016/j.proeng.2016.02.048

Keddar, B. (1985). Etude géologique et gitologique de l›indice de fer oolithique d›Aïn Babouche (Chéria, W. de Tébessa). M.Sc. Thesis, Université des Sciences et de la Technologie Houari Boumedienne, Alger.

Kimberley, M.M. (1979). Origin of oolitic iron formations. Journal of Sedimentary Petrology 49: 111-131. https://doi.org/10.1306/212F76D0-2B24-11D7-8648000102C1865D.

Kimberley, M.M. (1989). Exhalative origins of iron formations. Ore Geology Reviews 5: 13-145. https://doi.org/10.1016/0169-1368(89)90003-6

McGregor, F., Ramanaidou, E., Wells, M. (2010). Phanerozoic ooidal ironstone deposits – generation of potential exploration targets. Applied Earth Science 119: 60-64. https://doi.org/10.1179/037174510X12853354810660

Mutrux, J., Maher, H., Shuster, R., & Hays, T. (2008). Iron ooid beds of the Carolinefjellet Formation, Spitsbergen, Norway. Polar Research, 27(1), 28–43. doi:10.1111/j.1751-8369.2007.00039.x.

Nicholson, K. (1992). Contrasting mineralogical-geochemical signatures of manganese oxides; guides to metallogenesis. Economic Geology 87: 1253-1264. https://doi.org/10.2113/gsecongeo.87.5.1253

Nicolini, P. (1967). Remarques comparatives sur quelques éléments sédimentologiques et paléogéographiques liés aux gisements de fer oolithiques du Djebel Ank (Tunisie) et de Lorraine (France). Mineral. Deposita 2: 95-101. https://doi.org/10.1007/BF00206582

Pedersen, H.D., Postma, D., Jakobsen, R., Larsen, O. (2005). Fast transformation of iron oxyhydroxides by the catalytic action of aqueous Fe(II). Geochimica et Cosmochimica Acta 69: 3967-3977. https://doi.org/10.1016/j.gca.2005.03.016

Petranek, J., van Houten, F.B. (1997). Phanerozoic ooidal ironstones. Czech Geological Survey 7: 1-71.

Purser, B.H. (1980). Sédimentation et diagenèse des carbonates néritiques récents. Les éléments de la sédimentation et de la diagenèse. Tome 1., Editions technip, Paris.

Rudmin, M., Mazurov, A., Banerjee, S. (2019). Origin of ooidal ironstones in relation to warming events: Cretaceous-Eocene Bakchar deposit, southeast Western Siberia. Marine and Petroleum Geology 100: 309-325. https://doi.org/10.1016/j.marpetgeo.2018.11.023

Salama, W., El Aref, M.M. and Gaupp, R. (2013) Mineral evolution and processes of ferruginous microbialite accretion – an example from the Middle Eocene stromatolitic and ooidal ironstones of the Bahariya Depression, Western Desert, Egypt. Geobiology 11: 15-28. https://doi.org/10.1111/gbi.12011

Salama, W., El Aref, M., Gaupp, R. (2012). Mineralogical and geochemical investigations of the Middle Eocene ironstones, El Bahariya Depression, Western Desert, Egypt. Gondwana Research 22: 717-736. https://doi.org/10.1016/j.gr.2011.11.011

Salama, W., El Aref, M., Gaupp, R. (2014). Facies analysis and palaeoclimatic significance of ironstones formed during the Eocene greenhouse. Sedimentology 61: 1594-1624. https://doi.org/10.1111/sed.12106

Scholle, P.A. & Ulmer-Scholle, D.S. (2003). GRAINS: Non-skeletal Grains: Ooids, Pisoids, and Other Coated Grains. In: A Color Guide to the Petrography of Carbonate Rocks: Grains, textures, porosity, diagenesis. AAPG Memoir 77. https://doi.org/10.1306/M77973

Schweigart, H. (1965). Genesis of the iron ores of the Pretoria series, South Africa. Economic Geology 60: 269-298. https://doi.org/10.2113/gsecongeo.60.2.269

Siehl, A., Thein, J. (1989). Minette-type ironstones. Geological Society, London, Special Publications 46 : 175-193. https://doi.org/10.1144/GSL.SP.1989.046.01.16

Sonarem-Rudis. (1968). Recherches géologiques à Ain Babouche (Gisement de fer) effectuées en 1968. Sonarem, Algiers.

Sorby, H.C. (1849). On the Origin of the Cleveland Hill Ironstone. PYGS 3: 457-461. https://doi.org/10.1144/pygs.3.457

Taylor, S.R., McLennan, S.M. (1985). The Continental Crust: its Composition and Evolution. Blackwell Scientific Publications, Oxford.

Van Houten, F.B., Purucker, M.E. (1984). Glauconitic peloids and chamositic ooids - favorable factors, constraints, and problems. Earth-Science Reviews 20 : 211-243. https://doi.org/10.1016/0012-8252(84)90002-3

Vila, J.M. (1992). Carte géologique de l›Algérie à 1/50 000, feuille n° 265, Aïn Télidjène avec notice détaillée. Publication du Service de la Carte Géologique de l'Algérie, Boumerdes, Algeria 27pp.

Villain, F. (1902). Le gisement de minerai de fer oolithique de la Lorraine. Dunod, Paris.

Young, T.P. (1989). Phanerozoic ironstones: an introduction and review. Geological Society, London, Special Publications 46:9-25. https://doi.org/10.1144/GSL.SP.1989.046.01.02

Zaïer, A., Beji-Sassi, A., Sassi, S., Moody, R.T.J. (1998). Basin evolution and deposition during the Early Paleogene in Tunisia. Geological Society, London, Special Publications 132, 375–393. https://doi.org/10.1144/GSL.SP.1998.132.01.21